PERGAMON

International Journal of Heat and Mass Transfer 46 (2003) 367–379

International Journal of HEAT and MASS TRANSFER

www.elsevier.com/locate/ijhmt

On modelling the multidimensional coupled fluid flow and heat or mass transport in porous media

Anis Younes *

Laboratoire de Génie industriel, Université de la Réunion, 15 avenue René Cassin, BP 7151–97715, St Denis cedex 09 La Réunion, France

Received 25 July 2000; received in revised form 23 May 2001

Abstract

We consider the solution of coupled fluid flow and heat or mass transport in porous media. The aim of this work is to appraise mathematical assumptions used to decrease the CPU cost of the solution of these strongly non-linear coupled equations. This purpose is reached with a reduced model for which the term $\mathbf{q} \cdot \nabla \rho$ in the mass balance equation is neglected. Indeed, we show that this assumption allows an important reduction of computer time compared to the standard model. Moreover, contrarily to the Boussinesq approximation, no significant differences are found between the reduced and the standard model.

Model validation is carried out with a numerical code based on mixed and discontinuous finite elements. First, the Elder and the modified Evans and Raffensperger problems are simulated to test the different assumptions. Second, a simulation of two kinds of laboratory experiment is run without any calibration. For both computations, very similar results are obtained between the complete and the reduced fluid mass balance equations. Both models give numerical results in good agreement with the laboratory layered porous medium experiments. However, these models give less satisfactory results for the salt-pool problem.

Keywords: Non-linear systems; Partial differential equations; Numerical simulation; Boussinesq approximation; Laboratory experiments

1. Introduction

In this work, we consider the solution of coupled fluid flow and heat or mass transport in porous media. This can be encountered in a large number of environmental problems such as saltwater intrusion in exploited coastal aquifers, aquifers overlying salt formations, or geothermal reservoirs. It can also be encountered in industrial processes such as drying processes, heat pipe technologies or particulate materials processing.

For these problems, the fluid properties (density, viscosity) are dependent upon temperature and/or concentration. Therefore, fluid flow process occurring in porous media are described by strongly coupled non-linear systems of partial differential equations. Because of this non-linearity, there are no analytical models and we resort to numerical models to understand and predict solute and/or heat distribution in the domain.

A lot of numerical models have been developed. However, these models may lead to widely varying results in some cases [1–3]. For these problems, numerical difficulties arise essentially from the strong coupling among governing equations, the advection dominance of the transport equation and a large variability of the hydraulic conductivity of the porous medium.

In order to reduce the degree of coupling between the equations, and therefore reduce drastically the computer time, some assumptions can be employed [4,5]. Numerous 2D benchmarks (Henry, Elder, Salt Dome test cases) have been used to compare mathematical models and numerical codes accuracy.

* Tel.: +33-2-62-93-81-27; fax: +33-2-62-93-86-65.
E-mail address: anis.younes@univ-reunion.fr (A. Younes).

0017-9310/03/$ - see front matter
PII: S0017-9310(02)00264-8

Nomenclature

c_f	specific heat capacity of the fluid (J/kg/K)
c_s	specific heat capacity of the solid phase (J/kg/K)
$\mathbf{D}$	hydrodynamic dispersion tensor (m^2/s)
D_m	molecular diffusion coefficient of fluid (m^2/s)
g	the acceleration due to gravity (m/s^2)
$\mathbf{k}$	permeability tensor of the porous medium (m^2)
M	mobility ratio
Ng	gravity number
P	pressure ($kg/m/s^2$)
Q	sink/source term (1/s)
Q_T	heat source/sink function (W/m^3)
$\mathbf{q}$	specific discharge (Darcy velocity (m/s))
S_p	specific storage coefficient ($m\,s^2/kg$)
T	temperature (K)
ϕ	porosity
ρ	mass density of the fluid (kg/m^3)
ρ_s	density of the solid phase (kg/m^3)
ρ_1	maximum ($\omega = 1$) density of the fluid (kg/m^3)
ρ_0	reference ($\omega = 0$) fluid density (kg/m^3)
$(\rho c)_{fs}$	specific heat capacity of both fluid and solid phases (J/kg/K)
μ	dynamic viscosity of the fluid (kg/m/s)
μ_1	maximum ($\omega = 1$) viscosity of the fluid (kg/m/s)
μ_0	reference ($\omega = 0$) fluid viscosity (kg/m/s)
λ	hydrodynamic thermal dispersion tensor (W/m/K)
λ_f	thermal conductivity for the fluid phase (W/m/K)
λ_s	thermal conductivity for the solid phase (W/m/K)
δ_{ij}	Kronecker delta function
α_L	longitudinal dispersion length (m)
α_T	transversal dispersion length (m)
ω	mass fraction of solute
ω^*	solute mass fraction at sources

The aim of this work is to appraise these mathematical assumptions used to decrease the CPU cost. With this aim in view, we recall the most common mathematical models and some standard assumptions. We simulate two benchmarks that help for the selection of the mathematical model. Simulation of laboratory experiments allows the validation of the selected model.

All numerical experiments are carried out with a numerical code based on mixed and discontinuous finite elements methods, named TVDV-3D for Transport with Variable Density and Viscosity [6].

2. Mathematical models

The more common mathematical models of coupled fluid flow and heat or mass transport in porous media are based on the work of Bear [4]. The proposed model has been widely discussed by Hassanizadeh and Leijnse [7], Diersch and Kolditz [1] among others.

Flow, heat and mass transport in porous media are governed by four partial differential equations based on mass and energy conservation laws and Darcy's law.

The system of flow equations with varying density and viscosity is obtained from the mass conservation of the fluid:

$$\frac{\partial(\phi\rho)}{\partial t} + \nabla\cdot(\rho\mathbf{q}) = \rho Q \tag{1}$$

where ϕ is the porosity, ρ the mass density of the fluid, $\mathbf{q}$ the specific discharge (Darcy velocity) and Q the sink/source term and the generalized Darcy's law:

$$\mathbf{q} = -\frac{\mathbf{k}}{\mu}\cdot(\nabla P + \rho g \nabla z) \tag{2}$$

where μ is the dynamic viscosity of the fluid, $\mathbf{k}$ the permeability tensor of the porous medium and g the gravity acceleration.

Assuming that transport of solute through porous media is governed by the phenomena of convection, dispersion and molecular diffusion, and applying the mass conservation of solute, the transport equation can be written in terms of solute mass fraction ω:

$$\frac{\partial(\phi\rho\omega)}{\partial t} + \nabla\cdot(\mathbf{q}\rho\omega) - \nabla\cdot(\rho\mathbf{D}\cdot\nabla\omega) = \rho Q\omega^* \tag{3}$$

where ω^* is the solute mass fraction at sources.

The dispersion tensor $\mathbf{D}$ is given by a standard model accounting for both molecular diffusion and hydrodynamic dispersion [8]:

$$D_{ij} = (\alpha_T|\mathbf{q}| + \phi\tau D_m)\delta_{ij} + (\alpha_L - \alpha_T)\frac{q_i q_j}{|\mathbf{q}|} \quad i,j = 1,2,3 \tag{4}$$

where α_L and α_T are respectively the longitudinal and transversal dispersion length, D_m the molecular diffusivity, τ the tortuosity of the medium, and δ_{ij} the Kronecker delta function.

Assuming the immediate thermal equilibrium between the medium and the fluid, the heat transfer in porous media is governed by the phenomena of heat conduction and heat transport along with the flowing fluid. Applying the law of conservation of energy leads to the heat transfer equation written in terms of the temperature T as:

$$\frac{\partial((\rho c)_{\mathrm{fs}}T)}{\partial t}+\nabla\cdot(\rho c_{\mathrm{f}}\mathbf{q}T)-\nabla\cdot(\lambda_{\mathrm{e}}\nabla T)=Q_{\mathrm{T}} \tag{5}$$

where c_{f} is the specific heat capacity of the fluid, Q_{T} the heat source/sink function and $(\rho c)_{\mathrm{fs}}$ the specific heat capacity of the system formed by both fluid and solid phases defined as:

$$(\rho c)_{\mathrm{fs}}=(1-\phi)\rho_{\mathrm{s}}c_{\mathrm{s}}+\phi\rho c_{\mathrm{f}} \tag{6}$$

where ρ_{s} is the density of the solid phase and c_{s} the specific heat capacity of the solid phase. λ_{e} is the equivalent thermal conductivity of the fluid and porous medium. It includes dispersion in the fluid and heat conduction in both solid and fluid phases:

$$\lambda_{\mathrm{e},ij}=\rho c_{\mathrm{f}}\left[\alpha_{\mathrm{T}}|\mathbf{q}|\delta_{ij}+(\alpha_{\mathrm{L}}-\alpha_{\mathrm{T}})\frac{q_iq_j}{|\mathbf{q}|}\right]+[(1-\phi)\lambda_{\mathrm{s}}+\phi\lambda_{\mathrm{f}}]\delta_{ij}\quad i,j=1,2,3 \tag{7}$$

λ_{s} and λ_{f} are respectively thermal conductivity for the solid and the fluid phase.

Equations of flow, heat and mass transfer are coupled by the state equations that give the relationships for the fluid density and viscosity as functions of concentration and/or temperature. Generally the fluid density equation is expressed as a linear function of concentration and/or temperature. The dynamic viscosity of the fluid is regarded as an exponential function of concentration and/or temperature [4].

For both cases (mass transport or heat transport), the mathematical models are similar. They are based on the mass conservation of the fluid, the generalized Darcy's law and the convection dispersion equation of mass or heat transfer. Numerically the same techniques can be used for both cases. In the following, we detail coupling flow and mass transport in porous media, keeping in mind that similar procedures can be applied for coupled flow and heat transfer.

3. Standard assumptions for coupled flow and mass transport

In the following, we assume that the effect of temperature can be neglected, flow and mass transport equations are coupled by the following state equations:

$$\rho=\rho_0\left(1+\frac{\rho_1-\rho_0}{\rho_0}\omega\right),\quad \mu=\mu_0\left(\frac{\mu_1}{\mu_0}\right)^{\omega} \tag{8}$$

where ρ_1 and μ_1 are respectively, the maximum ($\omega=1$) density and viscosity of the fluid. ρ_0 and μ_0 are respectively the reference ($\omega=0$) fluid density and viscosity.

Considering, the solid matrix rigid and immobile and the porosity only a function of pressure P, combination of the generalized Darcy's law (2) and the mass balance equation of the fluid (1), leads to [6]:

$$\rho S_{\mathrm{p}}\frac{\partial P}{\partial t}+\phi\frac{\partial\rho}{\partial\omega}\frac{\partial\omega}{\partial t}+\nabla\cdot(\rho\mathbf{q})=\rho Q,$$
$$\mathbf{q}=-\frac{\mathbf{k}}{\mu}(\nabla P+\rho g\nabla z) \tag{9}$$

where S_{p} is the specific storage coefficient.

Using

$$h=\frac{P}{\rho_0 g}+z,\quad S=\rho_0 g S_{\mathrm{p}},\quad \mathbf{K}=\frac{\rho_0 g}{\mu}\mathbf{k} \tag{10}$$

The flow equations can be written in terms of equivalent head (h) as:

$$\mathbf{q}=-\mathbf{K}\left(\nabla h+\frac{\rho-\rho_0}{\rho_0}\nabla z\right) \tag{11}$$

$$\rho S\frac{\partial h}{\partial t}+\phi\frac{\partial\rho}{\partial\omega}\frac{\partial\omega}{\partial t}+\nabla\cdot(\rho\mathbf{q})=\rho Q \tag{12}$$

Using (1), the transport Eq. (3) can be written as:

$$\phi\rho\frac{\partial\omega}{\partial t}+\rho\mathbf{q}\cdot\nabla\omega-\nabla\cdot(\rho\mathbf{D}\cdot\nabla\omega)=\rho Q(\omega^*-\omega) \tag{13}$$

For transport problems, the non-linear dispersion equation, is very closed to the linear one [9].

To obtain the velocity field, pressure or solute distribution, we have to solve the strongly coupled system of the three (11)–(13) equations. In order to reduce the degree of coupling between these three equations, and therefore reduce the computer time, two standard assumptions have been proposed.

As stated by Bear [4], we consider that spatial variations of ρ in the mass balance equation (1) are much smaller than the local temporal ones. Therefore, in the first assumption, we consider that the term $\mathbf{q}\cdot\nabla\rho$ in the mass balance equation can be neglected. Eq. (1) is then replaced by:

$$\frac{\partial(\phi\rho)}{\partial t}+\rho\nabla\cdot(\mathbf{q})=\rho Q \tag{14}$$

This assumption consider that streamlines are mainly tangent to surfaces $\rho=$ constant. Eq. (12) becomes:

$$S\frac{\partial h}{\partial t}+\frac{\phi}{\rho}\frac{\partial\rho}{\partial\omega}\frac{\partial\omega}{\partial t}+\nabla\cdot(\mathbf{q})=Q \tag{15}$$

The second assumption is the Oberbeck–Boussinesq [10,11] approximation where density variations are neglected in the fluid mass balance. Indeed, the mass balance equation (1) is replaced by:

$$\frac{\partial\phi}{\partial t}+\nabla\cdot(\mathbf{q})=Q \tag{16}$$

This assumption implies that Eq. (12) can be replaced by:

$$S\frac{\partial h}{\partial t}+\nabla.(\mathbf{q})=Q \tag{17}$$

Under this assumption, Eqs. (11)–(13) are still coupled by the buoyancy term in the Darcy's law.

In the following, these three systems will be studied. The standard system formed by Eqs. (11)–(13) is referred as case 1. The second system, formed by Eqs. (11), (15) and (13) is referred as case 2. The last system, based on the Boussinesq approximation and formed by Eqs. (11), (17) and (13), is referred as case 3.

4. Numerical techniques

Numerous codes have already been developed, based on various numerical approaches (finite differences, finite elements) or combination of two distinct techniques like the method of characteristics and finite differences (e.g. [12]).

As stated by Diersch and Kolditz [1], success of numerical solution for variable density flow problems is essentially dependent on evaluating Darcy fluxes for a given discretization. To improve the accuracy of the velocity computation, we use the mixed hybrid finite elements approximation which is a good method to solve the fluid flow problem in porous media [13–15].

The idea of this method is to approximate simultaneously the state variable h and the flux $\mathbf{q}$. It provides continuous fluxes at inter-element boundaries throughout the field. Moreover, with the mixed formulation, the velocity is defined with the help of Raviart Thomas basis functions [16] and therefore a simple integration over the element gives the corresponding streamlines. Several studies [17–20] showed the superiority of the mixed finite element method with regard to the other classic methods. This superiority is outstanding for very variable or discontinuous hydraulic conductivity fields [17].

For the solute transport equation, we use a combination of discontinuous and mixed hybrid finite element methods. Upwind discontinuous finite elements coupled with a slope limiting technique [21] are well suited to solve the hyperbolic part of the transport equation. Indeed, this method introduce a very limited numerical diffusion even for very high Peclet number. For the dispersive part of the transport equation, mixed hybrid finite element method ensures an accurate computation of dispersive fluxes [22].

Dirichlet boundary conditions can be reproduced in a finite differences (average value over an element) or finite element (prescribed value at the node) way [9].

A detailed presentation in 2D of both methods applied to density driven flow simulations can be found in [6]. An explicit scheme is used for the convective part of the solute transport equation, an implicit scheme for its dispersive part [14]. Due to the explicit scheme, the Courant criterion has to be fulfilled which can lead to very small time steps. In order to reduce the CPU time, the computation of advection and dispersion is performed only for the elements where the mass exchange exceeds a prescribed value. Indeed, for each element, we compute the difference between the maximum and the minimum of mass fraction of its adjacent elements. The computation, for the new time step, is performed for this element only when this difference exceeds a prescribed value (10^{-4} in this work). To verify if this prescribed value is small enough we make a calculation of the total masse balance to estimate the total error in the domain. Therefore, masse fraction is computed only for regions where the gradient at the previous time step is non-equal zero (i.e. in the mixing zones). This can lead to a drastic reduction in CPU time.

In this simulator, TVDV-3D, the flow and transport equations are solved in a sequential way using a standard fixed point (Picard) scheme. The density of the new iteration is calculated from the mass fraction of the previous iteration step. The stopping criterion is based on the maximum value of the residual. The differences between this stopping criterion and a criterion based on the maximum change in the primary variables are discussed in [6].

5. In search of the adequate model

In order to choose the adequate model for coupling flow and mass transport in porous media, three versions of the numerical code, corresponding to the three cited cases, have been developed. The modified Evans and Raffensperger [23] problem and the Elder problem can help for the choice of the adequate model.

Recall that case 1 corresponds to the more coupled case and case 3 is the less coupled one. The discretization of the flow equation leads to an unsymmetrical matrix for case 1 and to a symmetrical matrix for cases 2 and 3.

5.1. The modified Evans and Raffenperger [23] problem

Evans and Raffensperger [23] defined a problem of salinity-driven convection in homogeneous domain to study errors inherent in the use of the Boussinesq assumption.

The domain is a vertical cross section of $1000 \times 1000\ \mathrm{m}^2$. Fluid and aquifer are assumed to be incompressible ($S = 0$). There are no sinks or sources in the domain. We conduct transient simulations with pressure and mass fraction equal to 0 inside the domain at $t = 0$. For cases 1, 2, and 3, the masse balance equation becomes:

$$\nabla \cdot (\rho \mathbf{q}) = -\phi \frac{\partial \rho}{\partial t} \quad \text{for case 1} \tag{18}$$

$$\nabla \cdot (\mathbf{q}) = -\frac{\phi}{\rho} \frac{\partial \rho}{\partial t} \quad \text{for case 2} \tag{19}$$

$$\nabla \cdot (\mathbf{q}) = 0 \quad \text{for case 3} \tag{20}$$

Originally, flow boundary conditions for the Evans and Raffensperger [23] problem are no flux for all boundaries. These boundary conditions are not consistent for cases 1 and 2. Since right terms in (18) and (19) are non-zero, we cannot obtain divergence free in the domain. To be consistent, we have to define a Dirichlet flow boundary condition in order to let fluid enter in the domain. Negative right terms in (18) and (19) imply an inflow at the imposed pressure boundary. For case 3, no flow boundary is obtained at this location. Therefore, differences between the three cases can be significant if we impose $\omega = 1$ at the location of the Dirichlet flow condition.

We conduct numerical experiments for two problems inspired from the Evans and Raffensperger [23] problem. Two different locations are used for the imposed pressure condition. Simulation parameters and boundary conditions are given in Tables 1 and 2.

Results of simulations at 300 and 600 years are shown in Fig. 1. For the problem 1, the results obtained for the three cases are similar. However for the second problem which is more sensitive ($\omega = 1$ at the location of the Dirichlet flow condition), case 3 based on the Boussinesq approximation fails to give good results. For this problem, the total mass in the domain at 600 years is greater for cases 1 and 2 than for case 3 (Fig. 1). Indeed, for the second problem, we have $\rho = 1200$ kg/m^3 at the imposed pressure boundary. Since at this location, there is an inflow with cases 1 and 2, we obtain more mass in the system than with case 3 which corresponds to zero flux at the Dirichlet flow boundary.

For both problems, results obtained from case 2 are identical to those from the standard case 1.

5.2. The Elder [24] problem

The experimental study of Elder [24] concern the flow produced by heating the base of a porous layer. It is a free convection problem where fluid flow is driven purely by fluid density differences. It involves total density variations of 20% which makes this problem a strongly coupled flow case. The equivalent solute transport of this thermal problem correspond to the salt water intrusion into uncontaminated aquifer by density driven convection. The parameters and boundary conditions for the pure solutal convection problem are given in Tables 3 and 4.

This test case has been widely studied ([2,5,6,25] among others). Results obtained for the three cases are plotted in Fig. 2.

As stated by Kolditz et al. [5], Fig. 2 shows that case (3), based on the Boussinesq approximation, can induce significant errors. It is interesting however to notice that, although these errors are important for 10 years results (Fig. 2(a)), they become insignificant for 20 years results (Fig. 2(b)).

As previously, no significant differences can be found between simulations performed for cases 1 and 2. The computations were run on a PW600 Digital Workstation with an alpha processor of 600 MHz. The fully coupled model (case 1) required more CPU time (720 s) because of its higher non-linear behaviour and because the discretisation of Eq. (12) leads to an unsymmetrical matrix. However, the numerical resolution of Eqs. (15) and (17) leads to a symmetrical matrix. The differences in CPU time between case 2 (464 s) and case 3 (393 s) are due to a higher coupling for case 2.

We conducted many other simulations for different problems using different boundary conditions. From these numerical experiments, it appears that the efficient model to solve the coupled fluid flow and mass transport equations, is described by equations of case 2. Indeed,

Table 1
Simulation parameters for the modified Evans and Raffensperger problem

Physical parameters	
Effective porosity	0.25
Hydraulic conductivity	10 m/year
Longitudinal dispersivity	30 m
Transverse dispersivity	10 m
Effective molecular diffusivity	10^{-4} m^2/yearr
Grid parameters	
Model scale	1000×1000 m^2
Number of elements	625

Table 2
Boundary conditions for problem 1 and problem 2

Boundary	Solute condition	Flow condition
Top	No solute flux	No fluid flux
Bottom	No solute flux	No fluid flux
Problem 1		
Left	$\rho = 1000$ kg/m^3 for $0 \leqslant y \leqslant 480$ m $\rho = 1200$ kg/m^3 for 480 m $\leqslant y \leqslant 1000$ m	No fluid flow
Right	No solute flux	No fluid flow for $0 \leqslant y \leqslant 960$ m $P = 0$ for 960 m $\leqslant y \leqslant 1000$ m
Problem 2		
Left	$\rho = 1000$ kg/m^3 for $0 \leqslant y \leqslant 480$ m $\rho = 1200$ kg/m^3 for 480 m $\leqslant y \leqslant 1000$ m	No fluid flow for $0 \leqslant y \leqslant 480$ m $P = 0$ for 480 m $\leqslant y \leqslant 520$ m No fluid flow for 480 m $\leqslant y \leqslant 1000$ m
Right	No solute flux	No fluid flow

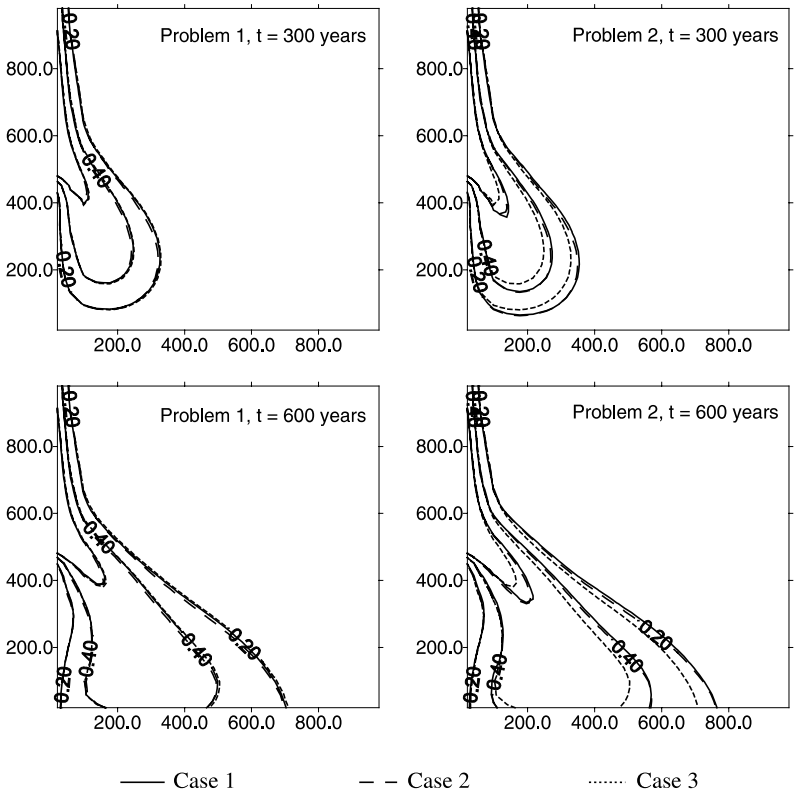

Fig. 1. Distribution of concentration at 300 and 600 years for problem 1 and problem 2.

Table 3
Simulation parameters for the Elder problem

Physical parameters	
Effective porosity	0.1
Hydraulic conductivity	$k_x = k_y = 4.845 \times 10^{-13}$ (m^2)
Longitudinal dispersivity	0 m
Transverse dispersivity	0 m
Effective molecular diffusivity	$D_m = 3.565 \times 10^{-6}$ (m^2 s^{-1})
Grid parameters	
Model scale	600×150 m^2
Number of elements	640

Table 4
Boundary conditions for the Elder problem

Boundary	Solute condition	Flow condition
Top	No solute flux for $0 \leqslant x \leqslant 150$ m	No fluid flux
	No solute flux for 450 m $\leqslant x \leqslant 600$ m	$P = 0$ at $x = 0$
	$\rho = 1200$ kg/m^3 for 150 m $\leqslant x \leqslant 450$ m	$P = 0$ at $x = 600$ m
Bottom	$\rho = 1000$ kg/m^3	No fluid flux
Left	No solute flux	No fluid flux
Right	No solute flux	No solute flux

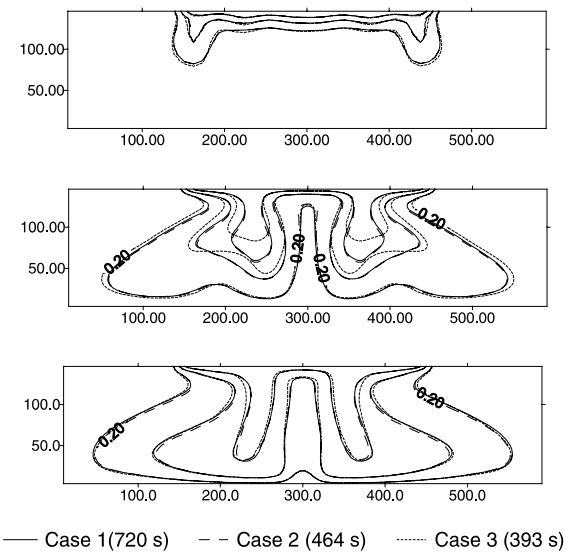

Fig. 2. Simulated concentration at 2, 10 and 20 years for the Elder problem.

with this model the CPU time can be 40% less than with the standard model without significant differences on results.

6. Model validation

Results of the model were confronted to 2D and 3D predictions of other numerical codes and also to laboratory experiment results [6,9,14,26]. In this part, we investigate the capacity of the model to simulate laboratory experiments of Loggia [27] for a layered medium and of Oswald [28] for the salt-pool problem.

Since the numerical results are to be compared with experimental data of Loggia [27] and Oswald [28], a brief description of their experimental setup will be given.

6.1. Effect of viscosity in stratified porous medium

Both porous medium heterogeneities and fluid density and viscosity affect solute transport in miscible fluid displacement. Loggia [27] experimentally studied both stable and unstable flow occurring in a layered medium. In this work, however, simulations are restricted to the stable flow field obtained when a more dense, viscous fluid (μ_+, ρ_+) displaces a less dense viscous one (μ_-, ρ_-). For this case, gravitational instabilities predominate at low velocities, and the viscosity stabilizing effect predominates at high velocities. The system will be stable or unstable depending on the velocity in relation to a critical velocity ([14,27,29–32] among others). In this work, are studied only the experiments with velocity much greater than the critical one (stable flow).

To characterize viscosity and density contrasts, we define the following parameters:

$$M = \frac{\mu_-}{\mu_+}, \quad Ng = kg\frac{\rho_+ - \rho_-}{q\mu_-} \tag{21}$$

where M is the mobility ratio and Ng the gravity number.

Laboratory experiments are done by Loggia [27]. A flow tank of 4.5 cm long, 4.5 cm wide, and 30 cm deep, is filled with a porous medium consisting of various sizes of industrial glass beads. Each layer is composed of a porous medium having a distinct conductivity and particle diameter. This required different conductivities and longitudinal dispersivities to be specified for different layers in the numerical simulation. The transverse dispersivity is chosen to be 10 times less than the longitudinal dispersivity. The different values for conductivity and longitudinal dispersivity used in the simulation are estimated from the average diameter of glass beads [27]. Table 5 presents the particle diameter, the conductivity, and the width for each layer. The same porosity ($\varepsilon = 0.4$) is used for the four layers.

Table 5
Porous media characteristics for Loggia problem

Layer	$\mathbf{k}_i$ (10^{-12} m^2)	d_i (10^{-6} m)	H_i (cm)
1	7.1	85	1.22
2	23.7	155	1.08
3	37.2	194	1.08
4	55.8	238	1.22

Table 6
Experimental data for Loggia problem

Experiment	1	2	3	4
q (cm/h)	9.89	9.89	4.95	4.95
$Ng\approx$	−0.09	0.8	0.65	0.33
$M\approx$	1	0.54	0.3	0.13

Many authors ([32–35] among others) have observed dependence between the dispersivity coefficient, the mobility ratio and the gravity number. Since the fluid displacement distance is small for Loggia experiments (<30 cm), the dispersivity coefficient is taken to be constant for all simulations.

Four experiments with different mobility ratio are simulated (Table 6). All experiments are done at a fixed temperature of 30 °C. A volumetric pump allows a fixed flow rate at the entry of the domain. Measured concentrations are based on acoustic process. It allows to obtain the average of concentration at five fixed altitudes (Z1 to Z5 in Fig. 3). Mixture of water–sucrose, and water–glycerin are used to obtain large variations of viscosity between the injected and the displaced fluid.

Boundary conditions for flow and solute transport are a fixed concentration and flow rate at the top and

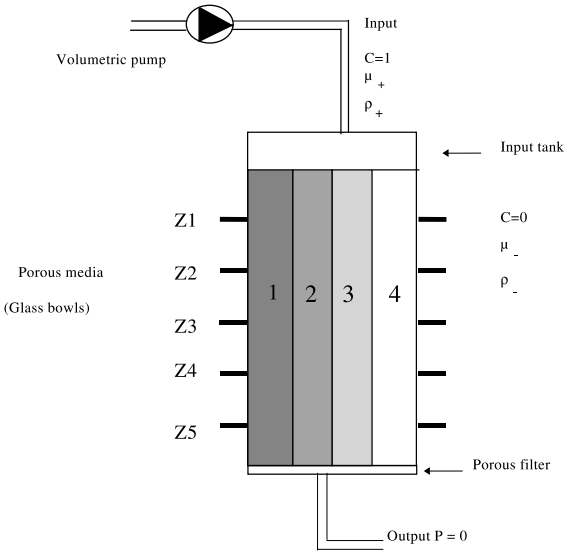

Fig. 3. Experimental setup (Loggia [27]).

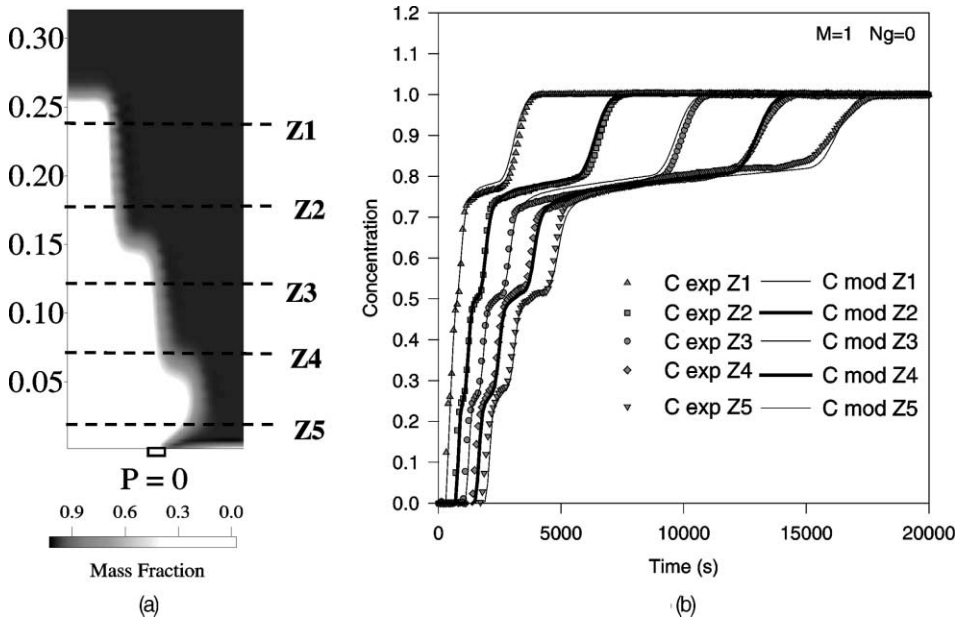

Fig. 4. (a) Distribution of concentration for experiment 1 at $t = 50$ min, (b) computed versus measured concentrations for experiment 1.

pressure equal to zero at the location of the draining pipe.

For the first experiment, there are no significant differences between the injected fluid properties (density and viscosity) and the displaced one. It corresponds to a tracer case. For this experiment, the solute advancement in each layer is proportional to the conductivity of this layer. It moves faster from high permeability zone (layer 4) to low permeability zone (layer 1). The effect of each layer can be distinguished in the results (Fig. 4(b)). The more the viscosity of the injected fluid increases (from experiment 1 to experiment 4) the less we can distinguish the effect of each layer separately.

Simulated concentrations and comparison between experimental and simulated average concentrations at different altitudes, are plotted for each experiment (Figs. 4–7). Small differences in terms of dispersivity occur between experimental and numerical results. The overall comparison shows good agreement between the numerical simulations and the laboratory experiments of Loggia [27] since all simulations are performed without any calibration.

Figs. 4(a) and 5(a) show that the average concentration obtained at level Z5 can be equal or greater than the one at level Z4. This phenomenon can be observed in Figs. 4(b) and 5(b). Cross transfer between layers occurs in the case of strong viscosity contrast (Fig. 7(a)). The effect of each layer cannot be distinguished. Therefore, the viscosity contrast damps out the effect of permeability.

To explain this phenomenon, let us consider two layered porous medium with $\mathbf{k}_2 = 2\mathbf{k}_1$ (Fig. 8). We assume that the two fluids present the same density. The injected fluid is, however, more viscous than the displaced one. Using Darcy's law (11), we see that the fluid velocity in each layer is proportional to $\mathbf{K}_i = (\rho_0 g/\mu)\mathbf{k}_i$. Zones (a) and (c) in Fig. 8 are assumed to be a long way from the mixing zone (b). For zones (a) and (c), we have the same viscosity in each layer. Therefore, the solute advancement in the layer (i) is proportional to its conductivity $\mathbf{k}_i$. Displacement occur without cross transfer between layers. However, in the mixing zone (b), because the viscosity of the injected fluid is greater than of the displaced one, $\mathbf{K_2}$ can than be smaller than $\mathbf{K_1}$. That's implies a transverse component of the velocity.

This phenomenon increases for large viscosity contrast as shown with streamlines plotted for the four experiments (Fig. 9).

6.2. The salt-pool problem

A 3D experiment, called the salt-pool experiment, conducted by Oswald [28] is used to verify the numerical code. A cube of $0.20 \times 0.20 \times 0.20$ m^3 is filled with industrial glass beads. The porous medium is then saturated with pure water. The cube contain five openings (squares) of dimension 0.001×0.001 m^2 (Fig. 10). The experiments were run in three steps:

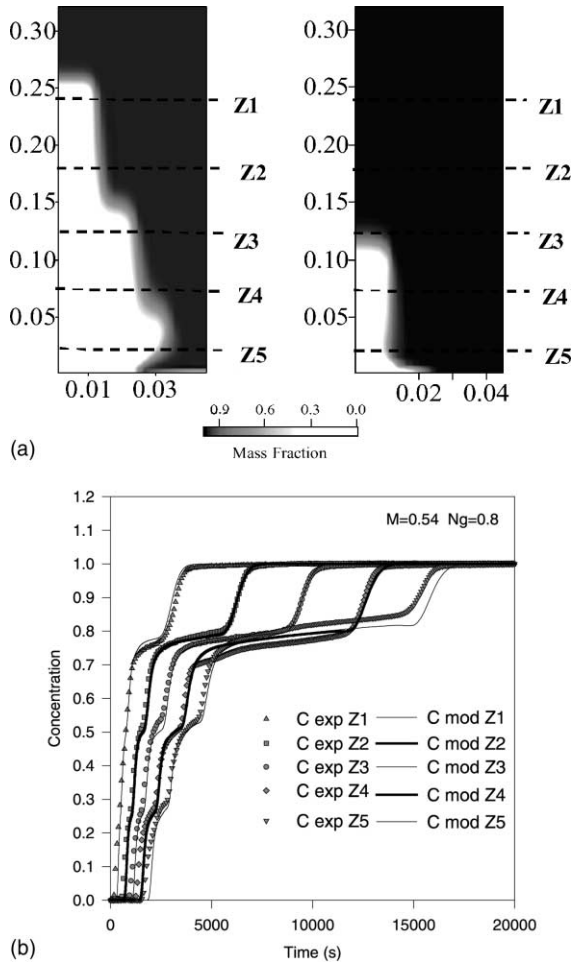

Fig. 5. (a) Distribution of concentration for experiment 2 at $t = 50$ and 200 min, (b) computed versus measured concentrations for experiment 2.

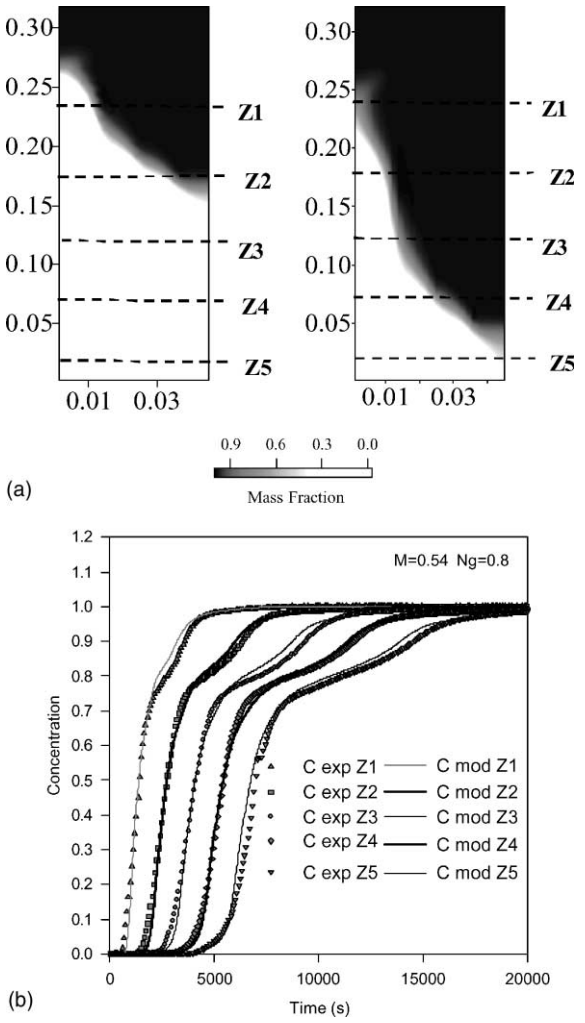

Fig. 6. (a) Distribution of concentration for experiment 3 at $t = 50$ and 100 min, (b) Computed versus measured concentrations for experiment 3.

- *Step 1:* injection of the salt water by the opening 5. The outflow is at openings 1 to 4.
- *Step 2:* no injection. All openings are closed.
- *Step 3:* injection at opening 4, outflow at opening 2, the others are closed.

Two experiments are simulated with the experimental conditions given in Oswald [28], Saltp-L with an input mass fraction of 1.0% and Saltp-D with an input mass fraction of 10%.

For steps 1 and 3, the flow rate is prescribed at the injection, a pressure equal to zero is prescribed at the outflow. Boundary conditions are given in [26,28]. Flow and transport parameters used for simulations (Table 7), are obtained by additional experiments done on columns or on the same cube with the same filling [28].

Several experiments have been performed by Oswald [28]. Simulation of the experiments performed with the highest concentration, is done with two versions of the numerical code, corresponding to cases 1 and 2.

Distribution of mass fraction in the cube, at the end of the step 1 ($t = 10$ min), the end of the step 2 ($t = 45$ min) and during the step 3 ($t = 63$ min), is plotted in Fig. 11. In this figure, are presented three numerical experiments corresponding to a tracer (EXP1), Saltp-L (EXP2), and Saltp-D (EXP3).

Contrarily to the tracer case, one can notice that dense brine tends to resist moving upwards and stagnates. This effect is more important for the Saltp-D experiment. However, it cannot be neglected for Saltp-L

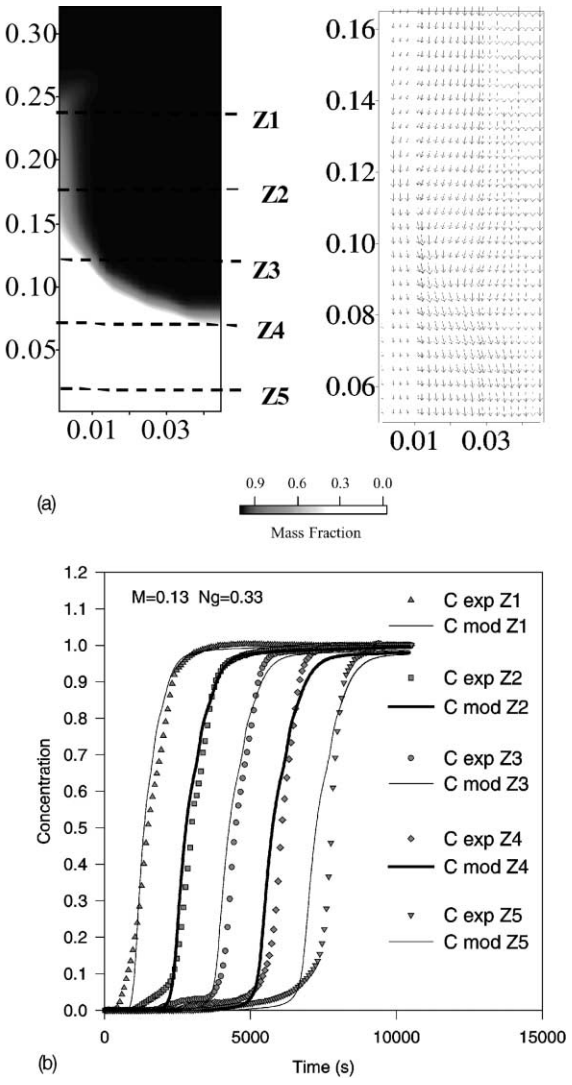

Fig. 7. (a) Distribution of concentration and velocity vector for experiment 4 at $t = 100$ min, (b) computed versus measured concentrations for experiment 4.

experiment even if the injected fluid present a mass fraction of only 1%.

Oswald [28] performed simulations of these experiments with a variety of codes to show the applicability of the experiments as a benchmark for verification of density driven flow codes. All these simulations gave quite different results and showed an overestimation of the maximum mass fraction for experiments Saltp-L (Fig. 12) and Saltp-D (Fig. 13). Results of TVDV-3D simulations are added in Figs. 12 and 13 for comparison. The maximum value is overestimated for Saltp -L and underestimated for Saltp-D by the TVDV-3D simulator. Both mathematical models provide very similar results [26].

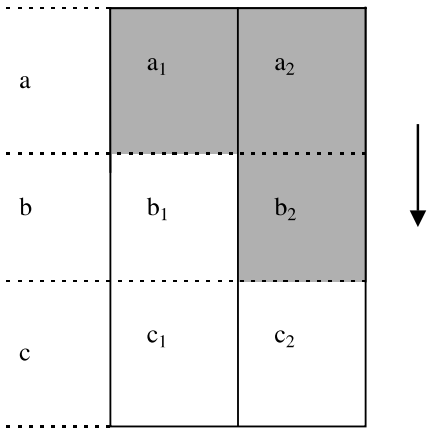

Fig. 8. Flow in two layered porous medium ($\mathbf{k_2} = 2\mathbf{k_1}$).

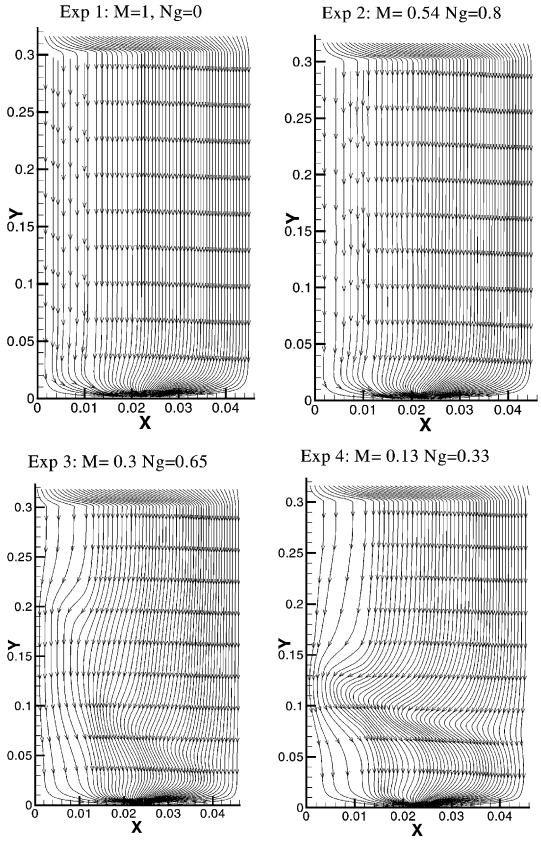

Fig. 9. Streamlines obtained for the four experiments.

The overall comparison shows that simulated results obtained with TVDV-3D are the closest to the experimental results (Figs. 12 and 13). Different computations have been run to improve the results [26]. Simulated

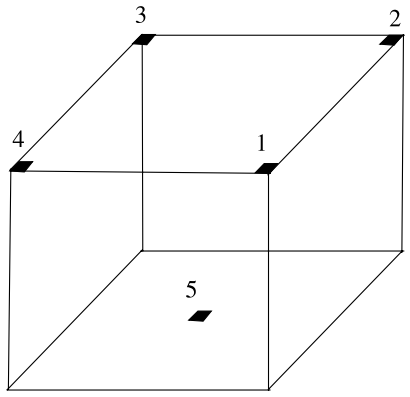

Fig. 10. The experimental cube and its openings.

Table 7
Flow and transport parameters used for the salt-pool problem

Permeability	9.8×10^{-10} (m^2)
Porosity	0.37
Longitudinal dispersivity	1.2×10^{-3} (m)
Transverse dispersivity	1.2×10^{-4} (m)
Molecular diffusion	8.7×10^{-10} (m^2/s)

results remain, however, different from experiments. Assuming that these experiments are reliable, they constitute a challenge for 3D density driven flow models.

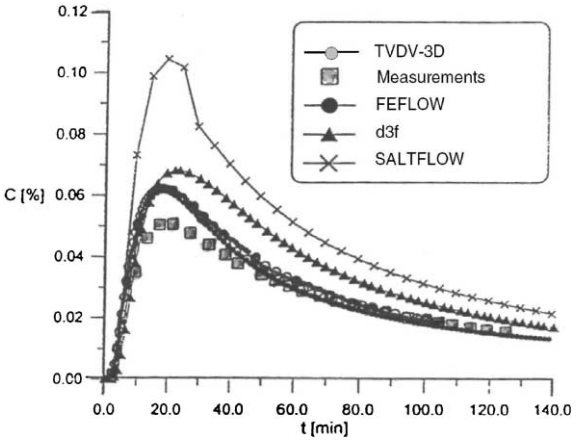

Fig. 12. Simulation of the Saltp-L (input mass fraction of 1.0%) experiment (modified from Oswald [28]). Results of TVDV-3D simulations are added for comparison.

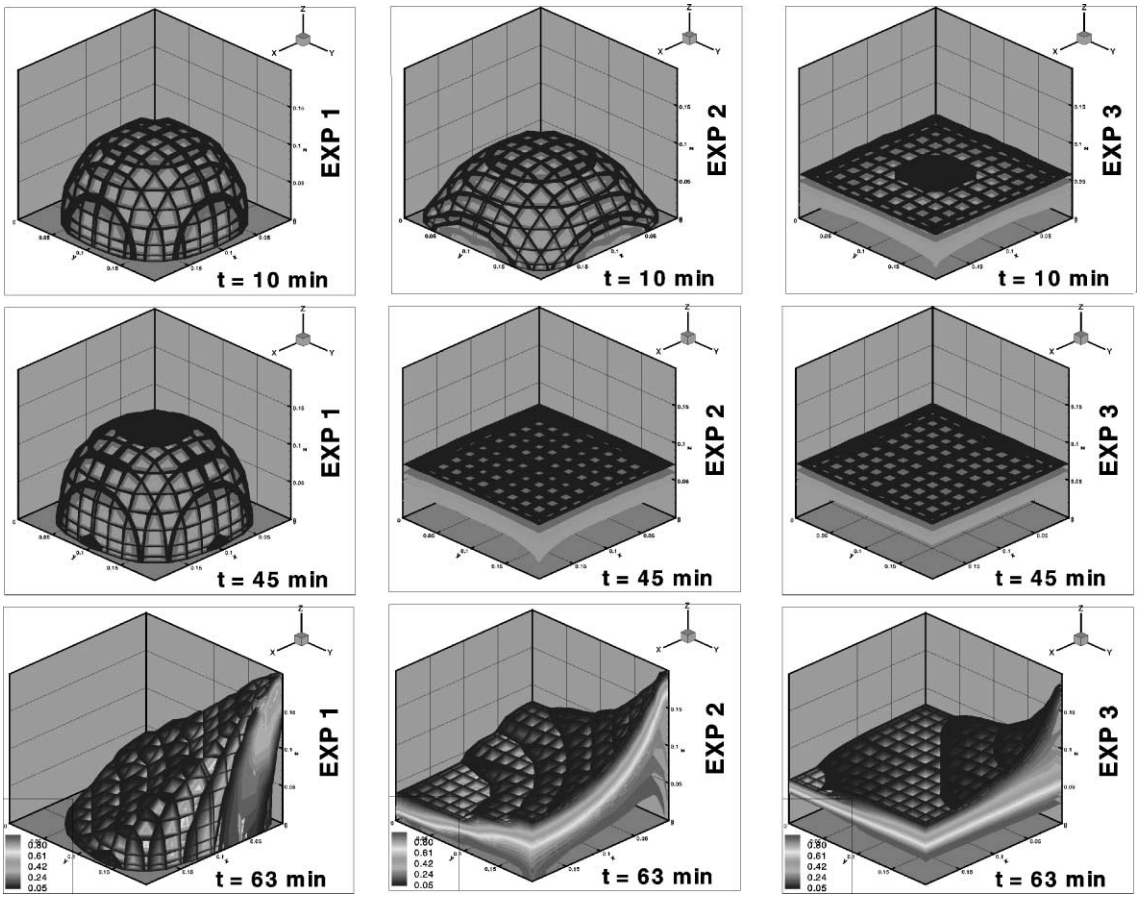

Fig. 11. Distribution of mass fraction in the cube for the salt-pool problem.

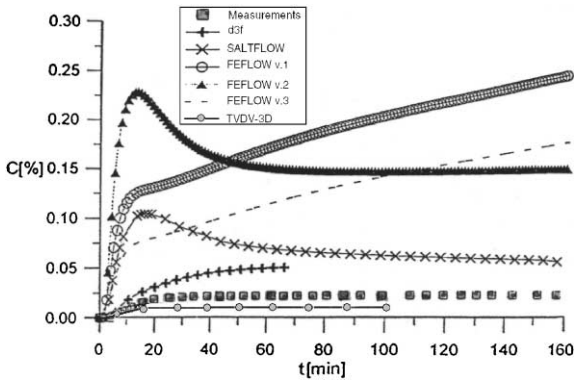

Fig. 13. Simulation of the Saltp-D (input mass fraction of 10%) experiment (modified from Oswald [28]). Results of TVDV-3D simulations are added for comparison.

7. Conclusions

Modelling flow and heat or mass transport in porous medium leads solving a strongly coupled system of partial differential equations. In order to reduce the degree of coupling between these equations, and therefore reduce the computer time, we have shown that the term $\mathbf{q} \cdot \nabla \rho$ in the mass balance equation (1) can be neglected. Indeed, with this assumption, the flow model leads to a symmetric matrix and the CPU time can be 40% less than with the standard approach. This assumption is implemented in numerical code based on mixed and discontinuous finite elements methods TVDV-3D.

The simulation of the modified Evans and Raffensperger [23] and the Elder [24] problems shows that results obtained with this assumption are identical to those obtained with the complete fluid mass balance equation.

This numerical mod el was also used to simulate laboratory experiments and predict the concentration distribution. Experimental study of the effect of large viscosity variations in layered porous medium was done by Loggia [27]. Simulation of these experiments without any calibration gives numerical results in good agreement with experimental data.

However, simulation of the salt-pool experiments done by Oswald [28] gives less satisfactory results.

References

[1] H.J. Diersch, O. Kolditz, Coupled groundwater flow and transport: 2. Thermoline and 3D convection systems, Adv. Water Res. 21 (1998) 401–425.

[2] C.M. Oldenburg, K. Pruess, Dispersive transport dynamics in a strongly coupled groundwater-brine system, Water Resour. Res. 31 (2) (1995) 289–302.

[3] Organization for Economic Cooperation and Development (OECD): 1988, The International Hydrocoin Project, level 1, Code verification, Rep. 71617, Paris.

[4] J. Bear, Dynamics of Fluids in Porous Media, Elsevier, New York, 1972.

[5] O. Kolditz, R. Ratke, H.J. Diersch, W. Zielke, Coupled groundwater flow and transport: 1. Verification of variable density flow and transport models, Adv. Water Res. 21 (1) (1997) 27–46.

[6] Ph. Ackerer, A. Younes, R. Mosé, Modeling variable density flow and solute transport in porous medium: 1. Numerical model and verification, Transport Porous Med. 35 (3) (1999) 345–373.

[7] M.S. Hassanizadeh, A. Leijnse, On the modeling of brine transport in porous media, Water Resour. Res. 24 (6) (1988) 321–330.

[8] G. De Marsily, Quantitative Hydrogeologiy, Academic, San Diego, California, 1986, pp. 230–247.

[9] A. Younes, Ph. Ackerer, R. Mosé, Modeling variable density flow and solute transport in porous medium: 2. Re-evaluation of the salt dome flow problem, Transport Porous Med. 35 (3) (1999) 375–394.

[10] A. Oberbeck, Ueber die Wärmelaitung der Flüssigkeiten bei Berücksichtigung der Strömung infolge von Temperaturdifferenzen, Ann. Phys. Chem. 7 (1879) 271–292.

[11] J. Boussineq, Recherches théoriques sur l'écoulement des nappes déau infiltrées dans le sol et sur le débit des sources, C.R.H Acad. J. Math. Pures Appliquées 10 (1903) 5–78.

[12] L.F. Konikow, W.E. Sanford, P.J. Campbell, Constant concentration boundary conditions: lessons from the HYDROCOIN variable-density groundwater benchmark problem, Water Resour. Res. 33 (10) (1997) 2253–2261.

[13] G. Chavent, J.E. Roberts, A unified physical presentation of mixed, mixed hybrid finite elements and standard finite difference approximations for the determination of velocities in water flow problems, Adv. Water Resour. 14 (6) (1991) 329–348.

[14] A. Younes, Modélisation de l'écoulement et du transport de masse en milieu poreux avec leséléments finis mixtes et discontinus. Prise en compte du contraste de masse volumique et de viscosité, Ph.D. thesis, Université Louis Pasteur-Strasbourg, France, 1998.

[15] A. Younes, Ph. Ackerer, R. Mosé, G. Chavent, A new formulation of the mixed finite element method for solving elliptic and parabolic PDE with triangular elements, J. Comput. Phys. 149 (1999) 148–167.

[16] P.A. Raviart, J.M. Thomas, A mixed finite method for the second order elliptic problems, in: I. Galligani, E. Magenes (Eds.), Mathematical Aspects of the Finite Element Method, Lecture Notes in Mathematics, Springer-Verlag, Berlin, 1977, pp. 292–315.

[17] L.J. Durlofsky, Accuracy of mixed and control volume finite element approximations to Darcy velocity and related quantities, Water Resour. Res. 30 (4) (1994) 965–973.

[18] R. Mosé, Application de la méthode deséléments finis mixtes hybrides et de la "marche au hasard" pour la modélisation de l'écoulement et du transport de masse en milieux poreux, Ph.D. thesis, Université Louis Pasteur-Strasbourg, France, 1990.

[19] R. Mosé, P. Siegel, P. Ackerer, G. Chavent, Application of the mixed hybrid finite element approximation in a ground-

water flow model: luxury or necessity?, Water Resour. Res. 30 (11) (1994) 3001–3012.
[20] A. Weiser, M.F. Wheeler, On convergence of block-centered finite differences for elliptic problems, SIAM J. Numer. Anal. 25 (1988) 351–375.
[21] E.F. Toro, Riemann solvers and numerical methods for fluid dynamics: a practical introduction, Springer-Verlag, Berlin, 1997.
[22] P. Siegel, R. Mosé, Ph. Ackerer, J. Jaffré, Solution of the advection dispersion equation using a combination of discontinuous and mixed finite elements, Int. J. Numer. Meth. Fluid 24 (1997) 595–613.
[23] D.G. Evans, J.P. Raffensperger, On the stream function for variable density groudwater flow, Water Resour. Res. 28 (1992) 2141–2145.
[24] J.W. Elder, Numerical experiments with a free convection in a vertical slot, J. Fluid Mech. 24 (1966) 823–843.
[25] C. Voss, W.R. Souza, Variable density flow and solute transport simulation of regional aquifers containing a narrow freshwater–saltwater transition zone, Water Resour. Res. 23 (10) (1987) 1851–1866.
[26] Ph. Ackerer, A. Younes, 1999, On modelling of density driven flow. International Conference on 'Calibration and Reliability in Groundwater Modelling: Coping with uncertainty', Zurich, 20–23 september 1999, IAHS Pub, pp. 13–22.
[27] D. Loggia, 1996, Etude par acoustique desécoulements de fluides miscibles en milieux poreux, Instabilités—hétérogèneités, Thèse de Doctorat de l'université Paris 7.
[28] S. Oswald, 1998, Dichteströmungen in porösen Medien: Dreidimensionale Experimente und Modellierung, Ph.D. Thesis, ETH Zürich (CH).
[29] S. Hill, Channelling in packed columns, Chem. Eng. Sci. 1 (1952) 247–253.
[30] F.J. Hickernell, Y.C. Yortsos, Linear stability of miscible displacements processes in poros media in the absence of dispersion, Stud. Appl. Math. 74 (1986) 93–104.
[31] M.A. Buès, A. Triboix, L. Zilliox, Stabilité des déplacements miscibles verticaux dans un milieu poreux en régime de dispersion mécanique, J. Theor. Appl. Mech. 6 (1987) 727–758.
[32] M.A. Buès, L. Zilliox, Déplacement miscible avec contraste de densité et de viscosité en milieu poreux. Identification des parametres de déplacement et stabilité en régime de dispersion mecanique, J. Hydrol. 120 (1990) 125–141.
[33] J. Tahar, Déplacement miscible:étude expérimentale de l'influence du contraste de viscosité, Communication No. 26, 3rd Colloq. Ass. Recherche Tech. Forage Prod., Pau, 1968.
[34] M.D. BenSalah, 1965, Influence des contrastes de viscosité et de densité sur le déplacement en milieu poreux de deux fluides miscibles. Thèse de docteur-ingénieur, Faculté des sciences de Toulouse.
[35] L.J.T.M. Kempers, H. Haas, The dispersion zone between fluids with different density and viscosity in a heterogeneous porous medium, J. Fluid Mech. 267 (1994) 299–324.